



Stability of Gerber systems with top-flange bracing

Vahab Esmaeili¹, Ali Imanpour², and Robert G. Driver³

Abstract

Cantilever-suspended-span construction using Gerber systems is widely used in North America for the roof framing in large single-story buildings. The key merits of such systems, as compared to conventional framing, include a more balanced moment distribution, simpler beam-to-column connections, and faster erection. However, the interaction between the back span and the cantilever can affect lateral-torsional buckling modes whose prediction requires considering a variety of parameters including the ratio between the cantilever and back span lengths, as well as loading and bracing conditions. From the design perspective, contemporary steel design standards such as the Canadian steel design standard and the US Specification for Structural Steel Buildings provide little guidance on the design of Gerber systems, which necessitates understanding the complex stability response of such systems. This paper aims to evaluate the stability of Gerber girders with a focus on the back span when the top flange is laterally restrained at discrete locations. A detailed finite-element model capable of considering material and geometric nonlinearities and imperfections is first developed and validated against available experimental data. The validated numerical model is utilized to obtain the lateral-torsional buckling modification factors associated with the back spans of 19,200 different single-overhanging girders with top-flange bracing under the free-to-warp conditions—as required by interaction methods. The results reveal that the current methods may lead to either overly conservative or unconservative predictions. Finally, artificial intelligence is applied to the results of the full database of numerical simulations to propose a model capable of predicting a lateral-torsional buckling modification factor for the back span of an arbitrary single-overhanging girder with top-flange bracing under the free-to-warp conditions based on only five dimensionless parameters.

1. Introduction

Cantilever-suspended-span construction is a popular structural roof system in North America for single-story buildings such as shopping centers, warehouses, and industrial buildings. In this system, the wide-flange girder of a typical bay extends beyond the column to support the girder of the adjacent bay, the span of which is shortened by the lengths of the cantilevers at each end. The ratio between the cantilever span and back span is of primary importance in the design process, as

¹ PhD Student, University of Alberta, Edmonton, AB <vahab@ualberta.ca>

² Assistant Professor, University of Alberta, Edmonton, AB <imanpour@ualberta.ca>

³ Professor, University of Alberta, Edmonton, AB <rdriver@ualberta.ca>

it affects the moment distribution in the structure (Figure 1). In other words, properly proportioning the cantilever span to the back span enables the designer to reduce the peak positive moments by allowing the structure to experience negative moments at the supports. Consequently, lighter and shallower girders are sufficient to carry the same loads with considerably smaller deflections. Furthermore, this system is statically determinate, and the simplicity of the beam-to-column connections results in faster fabrication and erection (Rongoe, 1996). All the above-mentioned benefits come at the cost of the challenges associated with the design of the Gerber system.

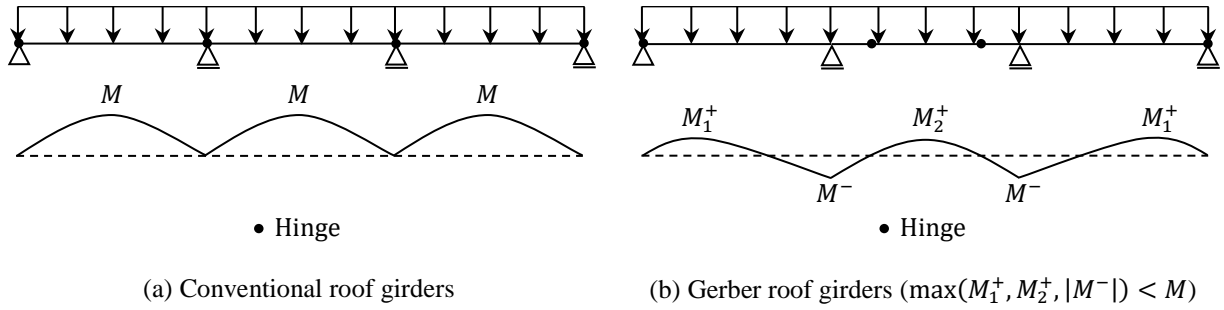


Figure 1: Bending moment diagrams associated with different types of roof girder

In Gerber construction, lateral and, potentially, torsional restraints are provided to the top flange of the girder by secondary framing members such as open-web steel joists (OWSJs). The attachment of the joist's extended bottom chord to the bottom flange of the main girder could also restrain the bottom flange laterally. Restraining the main girder either laterally or torsionally has been shown to be beneficial to the lateral-torsional stability of the whole system (Albert et al., 1992; Essa and Kennedy, 1993b). However, whether the current design procedures have succeeded in taking the restraints into account adequately is still a moot question.

To design overhanging girders, Nethercot (1973) recommended the effective length concept assuming a cantilever span and a back span of the same length, and without any lateral loads or restraints applied to the back span between supports. The tip of the cantilever was considered to be laterally restrained at the shear center. This method overlooked the fact that the length of the back span could affect the stability of the overhanging girder. Therefore, Kirby and Nethercot (1979) suggested the effective length of the cantilever segment be taken as not less than the length of the back span. It should be noted that the effective length concept was adopted by the SSRC guide (Galambos, 1998) without providing the above-mentioned restrictions.

Trahair (1983) proposed an interaction method to calculate the elastic lateral-torsional buckling (LTB) resistance for a double-overhanging girder whose cantilever segments are similar. Lateral restraints were assumed to be provided to the two supports, and top-flange and shear-center loadings were considered for the cantilever tips. This method used the buckling loads of the back span, under the assumption that it is free to warp at the ends, along with the buckling load of a cantilever built-in at the support, to obtain the capacity of the system through consideration of the interaction of adjacent members. It is noteworthy that the proposed method overestimates the buckling resistance for the cases with top-flange loading at the tip of the cantilever.

Essa and Kennedy (1994) proposed a method based on interaction buckling so as to obtain the elastic buckling resistance of overhanging girders when the cantilever segment is more critical

than the back span. The back span was assumed to be unrestrained between the supports with a single concentrated load applied at either the top flange or the shear center of the cantilever tip. In this method, the first step is to determine the buckling resistances of individual segments with no warping restraints at the supports—that is to say—without interaction. Equations were also provided to calculate the elastic critical moment of the cantilever segment with a free-to-warp condition at the support, whereas the elastic critical moment of the back span was determined using the provisions of the Canadian steel design standard of the day for conventional simply-supported beams with no restraints between the supports. Interaction factors were also presented for the cases with two different restraint conditions for the cantilever tip: free and laterally restrained at the top flange. For the case where lateral restraints are provided to both the top and bottom flanges at the cantilever tip, it was recommended that the procedures for interaction buckling of laterally continuous segments be used as presented in the SSRC guide (Galambos, 1998) or by Schmitke and Kennedy (1985). Moreover, when the back span is more critical than the cantilever segment, the cantilever could be neglected (Trahair, 1983).

Yura and Helwig (2010) investigated the buckling behavior of beams with reverse curvature bending, which represents a typical back span of an overhanging girder. The main challenge was to find the actual unbraced length of the beam under negative bending moments when restraints were provided only to the top flange. It was suggested that the inflection point, where the bending moment is zero, could not generally be considered a braced point. Furthermore, several LTB modification factors were proposed to adjust the uniform moment solution for special cases of beams with reverse curvature bending: cases with no restraints between the supports and those with continuous bracing on the top flange. Solutions were also presented for beams with bracing at one flange with a special focus on lateral bracing, torsional bracing, and composite construction.

From the presented literature review, it is deduced that interaction methods of obtaining the buckling resistance of overhanging girders require calculating the buckling resistances of individual segments without interaction in the first place. It should be noted that, in the Gerber system, the back span typically experiences both positive and negative bending moments (Figure 1(b)). However, in practice, only the top flange of the girder is restrained by secondary framing members such as OWSJs, while the bottom flange is unbraced. Thus, it is of primary importance that engineers be able to accurately determine the buckling capacity of a beam with reverse curvature bending and top-flange bracing. The main objective of this study is to propose a new LTB modification factor to estimate the elastic critical moment of an arbitrary beam with reverse curvature bending and top-flange bracing. To do this, first, a detailed finite-element model capable of considering material and geometric nonlinearities and imperfections is developed and validated against available experimental data (Essa and Kennedy, 1993a). Afterward, the effect of top-flange bracing on the stability of the back span with reverse-curvature bending is scrutinized, and the results are compared to the predictions by available design methods. Artificial intelligence (AI) is finally employed to propose a model for the prediction of appropriate LTB modification factors for different practical cases.

2. Numerical Simulation

The possibility of cross-sectional distortion is a critical consideration for evaluating the LTB of overhanging girders. In other words, such girders tend to experience coupled buckling modes with simultaneous distortion and deflection of the cross section due to their exposure to local and lateral buckles (Essa and Kennedy, 1994). In order to take this distortional buckling into account, S4R, a general-purpose 4-node shell element with reduced integration and a large-strain formulation—available in the *Abaqus* shell element library (Dassault Systèmes, 2017)—is employed in this study. Some of the important features of the selected element are as follows:

- S4R can provide robust and accurate solutions for structures best described by shear flexible shell theory, including thin and thick shell problems regardless of loading conditions;
- Never does S4R experience transverse shear locking;
- S4R uses reduced integration to form the element stiffness, which offers significant advantages in computational speed; and
- S4R is a first-order element with reduced integration and, consequently, prone to hour-glassing, although using a finer mesh or distributing point loads over multiple nodes can bring the issue under control.

Some of the distinguishing features of the present finite-element model are:

- The model is capable of considering material and geometric nonlinearities;
- The model is able to take account of residual stresses and initial geometric imperfections;
- The material properties do not have to be the same within the whole cross section, which could result in a more accurate model when the yield stress of the web is significantly higher than that of the flanges;
- The model is capable of considering distortion of both top and bottom flanges; however, distortion is not allowed for the top flange at load application points and for both top and bottom flanges at column locations so as to avoid hour-glassing; and
- The model accounts for different yielding patterns in the two flanges, thus accounting for the migration of the shear center location as the girder undergoes LTB.

3. Model Validation

To validate the numerical model developed in this study, experimental results by Essa and Kennedy (1993a) were used. They performed 33 full-scale tests using 11 W-shaped steel single-overhanging girders of two different cross sections: W360 × 39 and W310 × 39. The test set-up was designed so that five concentrated loads between the supports were spaced at 1219 mm and a single load was applied at the tip of a 1219-millimeter-long cantilever segment. Table 1 provides more details about the loading and restraint configurations of the test specimens. It is worthy of note that only 18 out of the 33 test specimens conform to the model proposed here in terms of boundary conditions.

Table 1: Loading and restraint configurations of test specimens (Essa and Kennedy, 1993a)

Test No.	Loading and restraint diagram	Section	Beam designation
1		W360 × 39	3B
2		W360 × 39	3B
3		W360 × 39	3B
4		W360 × 39	3B
7		W360 × 39	3A
9		W360 × 39	3K
10		W360 × 39	3K
11		W360 × 39	3K
12		W360 × 39	3K
13		W360 × 39	3K
14		W360 × 39	3K
15		W360 × 39	3K
16		W310 × 39	3V
17		W310 × 39	3V
20		W310 × 39	3T
21		W310 × 39	3T
22		W310 × 39	3T
28		W360 × 39	3H
<div style="display: flex; justify-content: space-between;"> <div> <p>○ Lateral restraint</p> <p>• Lateral and torsional restraint</p> <p>△, ▽ Reaction</p> </div> <div> <p>(a,b) Height of load application and height of lateral restraint above top flange, mm, if applicable</p> </div> </div>			

3.1 Material

Essa and Kennedy (1993a) tested a total of 22 coupons, 14 from the flanges and 8 from the webs, in uniaxial tension to determine the mean yield stresses and elastic moduli for the two W-shapes, presented in Table 2. It should be noted that elastic–perfectly plastic stress–strain curves are utilized for the numerical simulations, as the strain hardening effects become important at strains in excess of those experienced at buckling.

Table 2: Measured material properties (Essa and Kennedy, 1993a)

Section	E (GPa)	ν	$f_{y-Flange}$ (MPa)	f_{y-Web} (MPa)
W360 \times 39	204.5	0.3	287.9	317.8
W310 \times 39	209.3	0.3	352.2	367.4

3.2 Residual Stress

The sectioning method (Galambos, 1998) was used by Essa and Kennedy (1993a) in order to determine residual stresses in the flanges and webs of the two W-shapes. The reported results are presented in Figure 2.

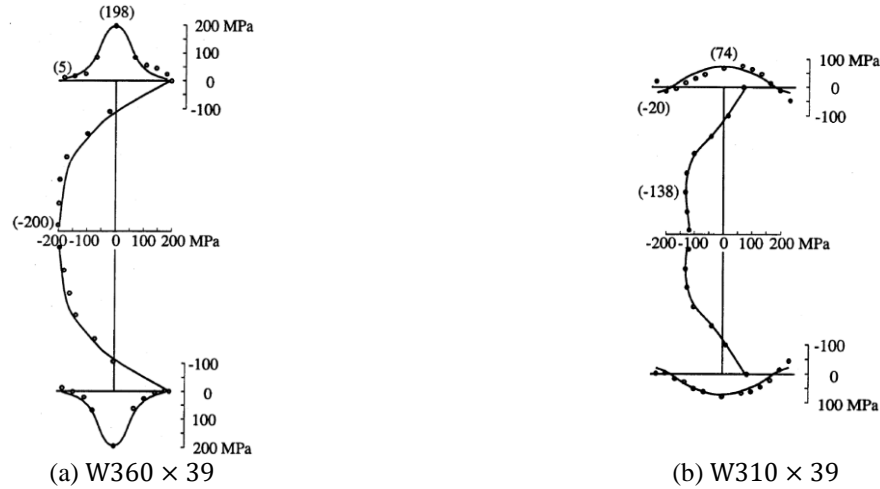


Figure 2: Residual stresses (Essa and Kennedy, 1993a)

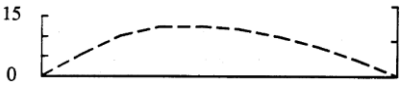

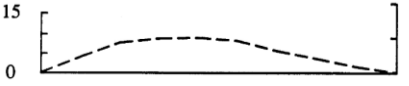
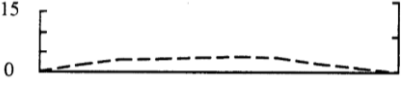
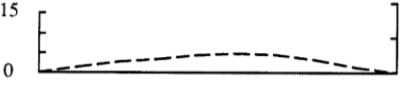
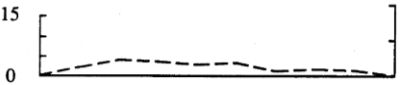
For the numerical simulations, the flanges and web are divided into several strips, and the residual stress is assumed to be constant across the width of each strip. Based on a sensitivity analysis, a mesh size of 10 mm is used, which results in 10 and 12 elements across the flange width and 24 and 22 elements along the web depth for the W360 \times 39 and W310 \times 39 sections, respectively. It is worthy of note that the number of strips is equal to the number of elements both across the flange width and along the web depth.

3.3 Initial Geometric Imperfection

For each test specimen, Essa and Kennedy (1993a) measured initial geometric imperfections including sweep of the shear center axis, twist, and camber at one-meter intervals. In this study, the initial sweep of each specimen (Table 3) is used to introduce initial geometric imperfections into the numerical model. To do this, first, the girder is analyzed under several displacement loads as measured and reported by Essa and Kennedy (1993a) at discrete locations. Afterward, the

deformed shape of the previous static analysis is introduced as the initial geometry of the girder for the nonlinear buckling analysis.

Table 3: Initial sweep of test specimens (Essa and Kennedy, 1993a)

Beam designation	Section	Initial sweep	
		δ , mm	δ/L
3B	W360 \times 39		.002 .000
3A	W360 \times 39		.002 .000
3K	W360 \times 39		.002 .000
3V	W310 \times 39		.002 .000
3T	W310 \times 39		.002 .000
3H	W360 \times 39		.002 .000

3.4 Boundary Conditions

In the experimental set-up, twist is prevented at both supports; however, no external warping restraints are applied. Figure 3(a) depicts the orientation of the axes associated with the girder model in *Abaqus*. According to the introduced system, the degrees of freedom are defined so that U_1 , U_2 , and U_3 represent translations in the 1, 2, and 3 directions, respectively; while UR_1 , UR_2 , and UR_3 are rotations about the 1, 2, and 3 directions, respectively. The applied boundary conditions, illustrated in Figure 3(b) and Figure 3(c), are interpreted as follows:

- The web is treated as a rigid body, the motion of which is governed by the motion of a single node where the web meets the bottom flange (reference node);
- All the nodes of each flange are constrained to the rotation of its midpoint around axis 3, which helps deal with the potential challenges caused by concentrated reaction forces; and
- Warping is not restrained externally.

At load application points, the boundary condition of the flange under the load is identical to that of the flanges at supports. Several lines with the mentioned boundary conditions are defined to ensure the distribution of point loads and reaction forces over a rectangular area with a length of 100 mm extending across the full width of the flange. Also, to adjust the height of the load application point and lateral restraint, separate reference points are defined at the specified level and rigidly connected to the associated flange (Figure 3(d)).

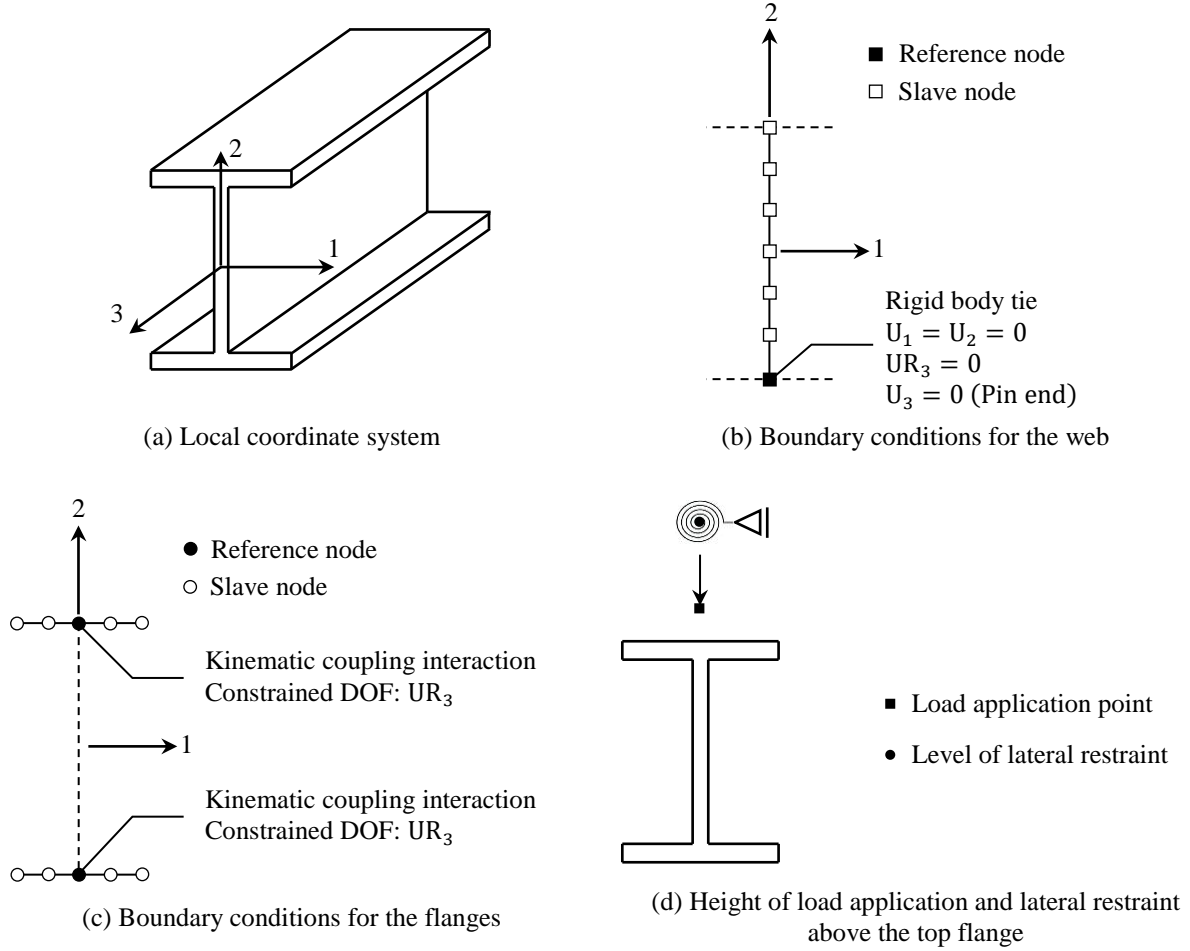


Figure 3: Modeling details of support locations and load application points

3.5 Analysis and Validation

The modified Riks method in *Abaqus* is adopted for the nonlinear buckling analysis of the test specimens. This method, which is also called the arc-length method, is an extremely efficient method for solving nonlinear systems of equations when one or more critical points are involved (Vasios, 2015). Loads are assumed to be proportional, and load–displacement response is considered to be smooth without any bifurcations (Dassault Systèmes, 2017). Table 4 summarizes the results from the experiment (Essa and Kennedy, 1993a) and the finite-element analyses (FEAs). The finite-element model is found to be capable of predicting the capacities of the test specimens with an acceptable accuracy. The mean ratio between the test results and the results from the numerical simulation is 0.99, with a coefficient of variation (CoV) of 10%.

Table 4: Finite-element model validation results

Test No. (Essa and Kennedy, 1993a)	P (kN)		Test/FEA	Instability Type	Beam Designation (Essa and Kennedy, 1993a)
	Test (Essa and Kennedy, 1993a)	FEA			
1	75.1	76.8	0.98	Elastic	3B
2	78.9	84.3	0.94	Elastic	
3	77.1	82.5	0.93	Elastic	
4	104.9	114.6	0.92	Elastic	
7	76.1	76.5	1.00	Elastic	3A
9	35.5	42.8	0.83	Elastic	3K
10	41.1	36.7	1.12	Elastic	
11	44.1	36.7	1.20	Elastic	
12	46.4	45.3	1.02	Elastic	
13	48.2	46.1	1.05	Elastic	
14	132.4	132.6	1.00	Inelastic	
15	136.8	137.1	1.00	Inelastic	
16	84.0	104.2	0.81	Elastic	3V
17	77.6	86.3	0.90	Elastic	
20	52.7	48.6	1.08	Elastic	3T
21	154.5	155.2	1.00	Inelastic	
22	133.3	143.7	0.93	Elastic	
28	128.8	121.2	1.06	Inelastic	3H
Mean			0.99		
Standard Deviation (SD)			0.09		
Coefficient of Variation (CoV)			0.10		

4. Buckling resistance of back span with top-flange bracing

The stability response of the Gerber system with emphasis on the back span with top-flange bracing is examined using the validated finite-element model. For this purpose, the performance of three LTB modification factors in estimating the elastic critical moment of the back span is first evaluated. A database of numerical simulations are then developed and used to propose a more efficient LTB modification factor with the aid of AI.

4.1 Available LTB modification factors

As mentioned in Section 1, Essa and Kennedy (1994) proposed an interaction equation for the buckling capacity of overhanging girders with a concentrated load at the cantilever tip and fork supports. This method rests on the assumption that the back span would be unrestrained between the supports (Ziemian, 2010). In this method, the elastic critical moment of the back span subject to shear-center loading was given by

$$M_{cr} = \frac{\omega_2 \pi}{L_b} \sqrt{EI_y GJ + \left(\frac{\pi E}{L_b}\right)^2 I_y C_w} \quad (1)$$

where E and G are the elastic modulus and shear modulus of steel, respectively; I_y is the moment of inertia about the weak axis of the cross section; J and C_w represent the St. Venant torsional constant and warping torsional constant, respectively; L_b is the length of the back span; and, ω_2 is the LTB modification factor, which accounts for various bending moment gradients along the back span and is calculated using the following equation in accordance with CSA S16-19 (CSA, 2019):

$$\omega_2 = \frac{4M_{max}}{\sqrt{M_{max}^2 + 4M_a^2 + 7M_b^2 + 4M_c^2}} \leq 2.5 \quad (2)$$

In Equation (2), M_a , M_b , and M_c are the absolute values of moment at the quarter point, centerline, and three-quarter point of the back span, respectively; and, M_{max} is the absolute value of the maximum moment in the back span.

According to AISC 360-16 (AISC, 2016), ω_2 should be replaced by C_b – which is calculated as follows:

$$C_b = \frac{12.5M_{max}}{2.5M_{max} + 3M_a + 4M_b + 3M_c} \quad (3)$$

Equation (1) cannot be used when the loads are applied at the top-flange level (Essa and Kennedy, 1993a). Thus, more sophisticated finite-element programs must be used to obtain the elastic critical moment of the back span.

Yura and Helwig (2010) proposed another LTB modification factor for gravity loaded rolled I-section beams with the top flange laterally restrained (AISC, 2016). This factor is defined as

$$C_{b-YH} = 3.0 - \frac{2}{3} \left(\frac{M_1}{M_o} \right) - \frac{8}{3} \left[\frac{M_{CL}}{(M_o + M_1)^*} \right] \quad (4)$$

in which M_o is the moment at the end of the back span that gives the largest compressive stress in the bottom flange; M_1 is the moment at the other end of the back span; M_{CL} is the moment at the centerline of the back span; and, $(M_o + M_1)^*$ is equal to M_o if M_1 is positive and causes tension on the bottom flange.

4.2 Data generation

Figure 4 demonstrates the configuration of the beams to be analyzed. It is assumed that the bending moment at one end is always equal to zero, indicative of a single-overhanging girder. In Figure 4,

- P_i refers to the i -th point load on the beam when counted from left to right (all point loads are assumed to be of the same value);
- L_b denotes the length of the beam;
- s represents the joist spacing;
- n equals the number of point loads on the beam plus 1;
- M_B is the bending moment at the centerline;
- M_F signifies the bending moment at the right support (fulcrum); and,
- R is defined as the ratio between M_B and M_F .

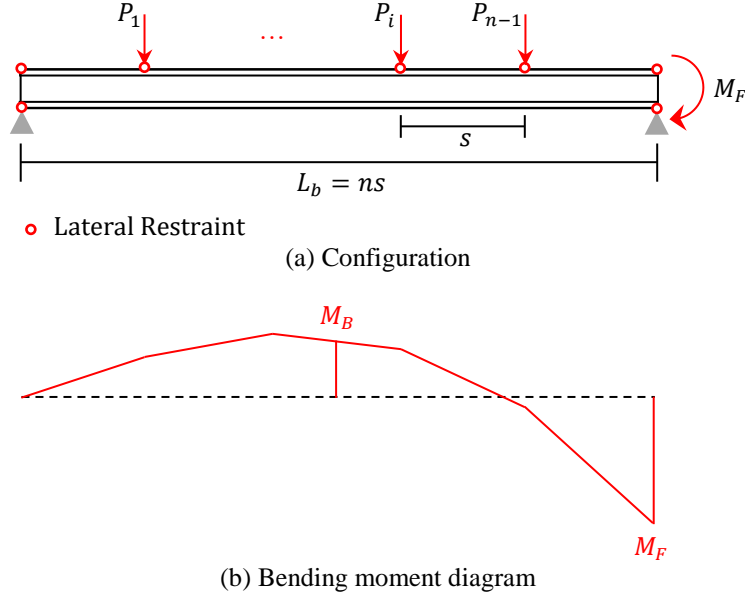


Figure 4: Typical beam with reverse curvature bending

To ensure the inclusiveness and practicality of the dataset, the following ranges are taken into account for L_b , n , and R .

$$L_b = \{8000, 9000, 10000, 11000, 12000\} \text{ mm} \quad (5)$$

$$n = \{5, 6, 7, 8, 9, 10\} \quad (6)$$

$$R = -2.5 + 0.2i \quad (i = \{0, 1, 2, \dots, 14, 15\}) \quad (7)$$

Also, 40 standard steel W-shapes, including the most common cross sections utilized in Gerber construction, are considered. The selected sections along with the class of each (CSA, 2019) are presented in Table 5. Therefore, the selected cross sections in combination with the ranges introduced by Equations (5), (6), and (7) provide 19,200 unique finite-element problems to be solved. The previously-validated finite-element model is utilized to obtain the elastic critical moment of each structure from an eigenvalue buckling analysis in *Abaqus*.

Table 5: Selected cross sections

Cross Section	Class	Cross Section	Class	Cross Section	Class	Cross Section	Class
W250x67	1	W530x123	1	W530x101	1	W610x113	1
W310x74	1	W460x82	1	W610x140	1	W610x195	1
W410x85	1	W410x60	1	W610x82	1	W610x101	1
W310x143	1	W530x74	1	W530x92	1	W610x174	1
W460x68	1	W460x52	1	W460x128	1	W610x155	2
W460x97	1	W460x74	1	W610x241	1	W840x193	1
W530x138	1	W530x109	1	W610x125	1	W920x223	1
W460x89	1	W610x92	1	W530x82	2	W1000x371	1
W530x85	1	W460x144	1	W610x217	1	W840x299	1
W460x60	1	W530x66	1	W460x113	2	W1100x390	1

4.3 Performance assessment of the available LTB modification factors

Knowing M_{cr} from the performed FEAs, the LTB modification factors are back-computed from Equation (1) and introduced as $C_{b\text{-FEA}}$. Also, for each case, the three different available LTB modification factors are calculated through Equations (2), (3), and (4). Figure 5 demonstrates the performance of different methods in predicting the LTB modification factor of a back span with top-flange bracing at discrete locations. For each case, the mean ratio between the LTB modification factor obtained from the numerical simulation and the approximate one calculated using either Equations (2), (3), or (4) is reported, along with the associated coefficient of variation.

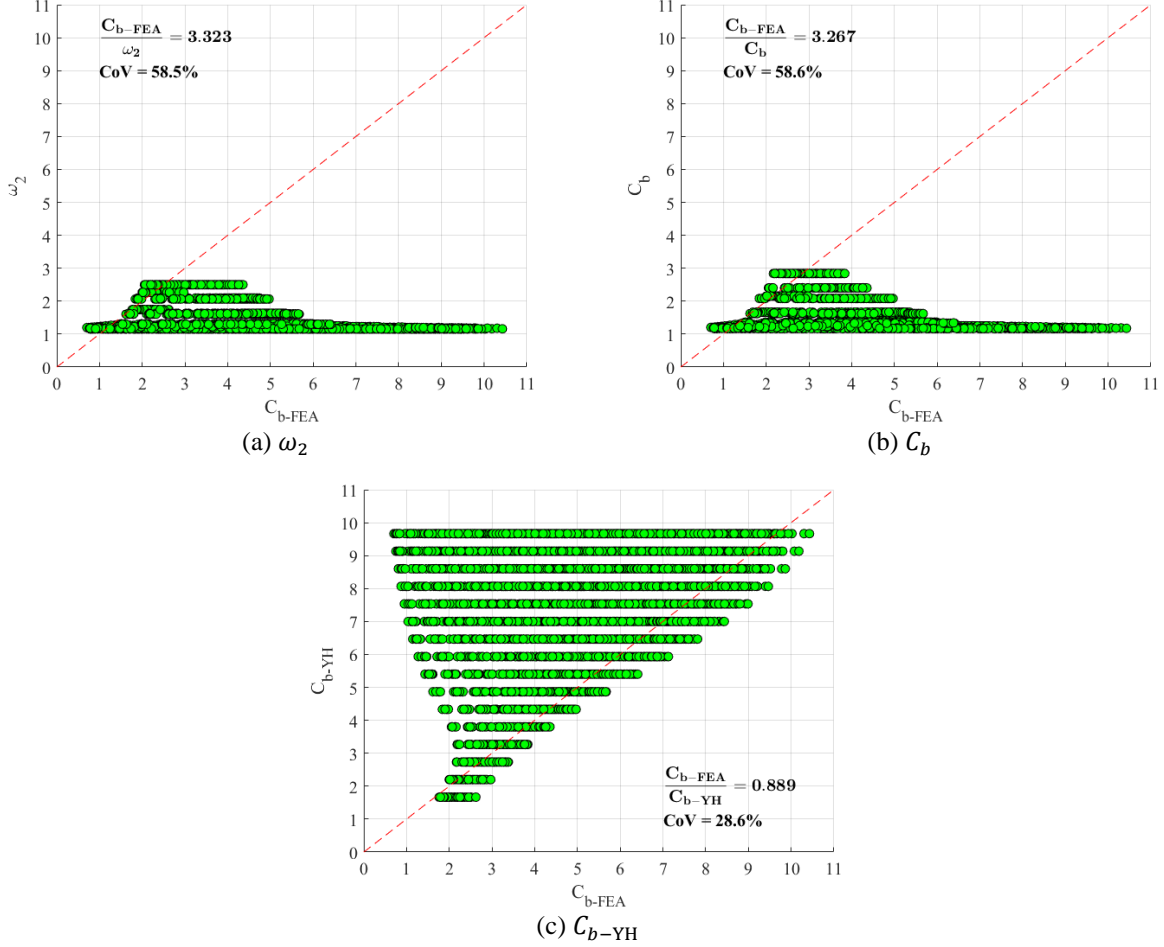


Figure 5: Performance of LTB modification factors

The mean FEA/approximate ratios for Equations (2) and (3) are 3.323 and 3.267, respectively, suggesting that they are too conservative for general use when the back span is laterally restrained at the top flange. This could be accounted for by the fact that the factors given by CSA S16-19 (CSA, 2019) and AISC 360-16 (AISC, 2016) have been developed based on the assumption that the beam is entirely unbraced between the two ends. Therefore, the beneficial effect of top-flange bracing is neglected for the cases of the present study and, consequently, conservative values are expected. Moreover, Equations (2) and (3) have been calibrated for the cases with shear-center loading, whereas the present cases are loaded at the top-flange level. Thus, without the

destabilizing effect of top-flange loading, the numerical LTB modification factors for the present cases would be even greater.

The mean FEA/approximate ratio for Equation (4) is 0.889, which implies that the equation proposed by Yura and Helwig (2010) can be unconservative. It should be noted that Equation (4) is based on the assumption that the entire top flange is laterally restrained, while for the present study the top flange is laterally restrained at discrete locations.

4.4 Model prediction

The database generated in Section 4.1 is analyzed so as to propose a model capable of predicting the elastic critical moment of the back span of any arbitrary single-overhanging girder. For this purpose, AI is used to model the relationship between the LTB modification factor for back span in the Gerber system and several features of the system.

4.4.1 Support vector machines for regression

Regression is defined as the task of modeling the relationship between a dependent variable and one or more independent variables. Support vector machines are among the best kernel learning algorithms (Rivas-Perea et al., 2013), a variant of which – known as support vector regression (SVR) – has been applied successfully to regression problems. This algorithm is capable of solving highly nonlinear problems through mapping the input space to a higher-dimensional space. As illustrated by Figure 6, SVR attempts to fit a tube of width ϵ to the data (Mohri et al., 2018) to create two distinct sets of points: inside and outside the tube. The points falling inside the tube incur no loss, whereas those falling outside the tube are penalized based on their distance from the predicted function.

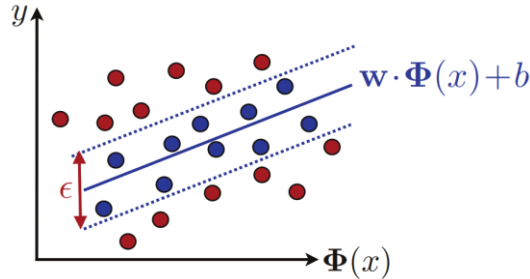


Figure 6: Support vector machines for regression (Mohri et al., 2018)

A hypothesis set of linear functions is considered as

$$\mathcal{H} = \{x \mapsto \mathbf{w} \cdot \Phi(x) + b : \mathbf{w} \in \mathbb{R}^N, b \in \mathbb{R}\} \quad (8)$$

where Φ is the feature mapping corresponding some positive definite symmetric kernel K . Therefore, the optimization problem for SVR can be expressed as follows (Mohri et al., 2018):

$$\min_{\mathbf{w}, b} \frac{1}{2} \|\mathbf{w}\|^2 + C \sum_{i=1}^m |\mathcal{Y}_i - (\mathbf{w} \cdot \Phi(x) + b)|_{\epsilon} \quad (9)$$

where $|\cdot|_\epsilon$ is called the ϵ -insensitive loss. The optimization problem is transformed into a dual problem by introducing Lagrange multipliers α and α' , which are meant to be determined through quadratic programming (QP). Finally, SVR returns hypothesis h as

$$\forall x \in \mathcal{X}, h(x) = \sum_{i=1}^m (\alpha'_i - \alpha_i) K(\mathbf{x}_i, \mathbf{x}) + b \quad (10)$$

Note that any positive definite symmetric kernel is permitted to be used with SVR (Mohri et al., 2018). One of the most frequently used nonlinear kernels in applications is Gaussian kernel or radial basis function (RBF), defined as

$$\forall \mathbf{x}, \mathbf{x}' \in \mathbb{R}^N, K(\mathbf{x}, \mathbf{x}') = \exp\left(-\frac{\|\mathbf{x}' - \mathbf{x}\|^2}{2\sigma^2}\right) \quad (11)$$

4.4.2 Feature selection

Among many potential features, including sections properties, length of the back span, joist spacing, and bending moment gradient, only five dimensionless features are selected as follows:

- $\frac{b}{2t}$, which is indicative of the flange slenderness for W-shapes, where b is the overall width of the flange and t denotes its thickness;
- $\frac{I_x}{I_y}$, which is an index of the difference between the strong- and weak-axis geometric stiffness of the girder;
- R , which is the ratio between the bending moment at the centerline of the back span and that at the fulcrum, indicative of the bending moment gradient along the back span;
- n , which is the number of point loads on the back span plus one, mostly indicative of joist spacing and the distribution of lateral restraints along the back span; and
- $X = \frac{\pi}{L_b} \sqrt{\frac{EC_w}{GJ}}$, which is principally a torsional parameter reflective of the ratio between the warping and St. Venant torsional stiffnesses, and for steel the ratio between E and G is assumed to be constant.

The correlation matrix associated with these five features and the target, which is the modification factor obtained using the finite-element model, is presented in Table 6. Each correlation coefficient, which is a number between -1.0 and 1.0, refers to the degree to which a pair of attributes are related. The correlation is computed as

$$r = \frac{\sum (x_i - \bar{x})(y_i - \bar{y})}{\sqrt{\sum (x_i - \bar{x})^2 \sum (y_i - \bar{y})^2}} \quad (12)$$

where x and y are two sets of variables; and, \bar{x} and \bar{y} are their mean values, respectively. As presented in Table 6, the correlation coefficients related to most pairs of features are either zero or relatively small. This could be construed as a desirable feature selection since one of two highly correlated features is less likely to be helpful in the training process due to their probable strong

similarity. Furthermore, there is a meaningful correlation between each feature and the target, which seems promising as well.

Table 6: Heat map for selected features and the outcome variable

	$\frac{b}{2t}$	$\frac{I_x}{I_y}$	R	n	X	C_{b-FA}
$\frac{b}{2t}$	1.00	-0.17	0.00	0.00	0.33	-0.10
$\frac{I_x}{I_y}$	-0.17	1.00	0.00	0.00	0.03	0.13
R	0.00	0.00	1.00	0.00	0.00	-0.63
n	0.00	0.00	0.00	1.00	0.00	0.08
X	0.33	0.03	0.00	0.00	1.00	-0.52
C_{b-FA}	-0.10	0.13	-0.63	0.08	-0.52	1.00

It is also important to ensure that each feature enjoys an appropriate frequency distribution over the dataset. Figure 7 shows the probability distribution for each feature, along with its mean value and standard deviation. It is observed that the features are well-distributed and mostly include the values encountered in practice.

4.4.3 Proposed model

The dataset is divided into two different subsets: 60% for training the model and 40% for validation. The validation set is used in a robust multiple hold-out performance calculation. A Gaussian kernel or RBF is employed so as to train the model through SVR algorithm. The optimal values for the kernel gamma ($\frac{1}{2\sigma^2}$) and the complexity constant (C) are found to be 0.5 and 10, respectively. The production model is finally created by training a model with the same parameters on the combined training and validation sets. Table 7 summarizes the details of the production model, and Figure 8 demonstrates the excellent performance of the model in predicting the elastic critical moment of a back span with top-flange bracing at discrete locations as expected to be encountered in practice.

Table 7: The proposed model for the prediction of LTB modification factors

Kernel Type	Gaussian (RBF)
Total number of support vectors	15,000
Bias (Offset)	3.386
$w(b/2t)$	-5.697
$w(I_x/I_y)$	53.661
$w(R)$	-97.471
$w(n)$	57.372
$w(X)$	-159.808

It is of crucial importance that engineers be fully aware of the limitations or underlying assumptions of different methods. The proposed model in this study rests on the following assumptions:

- The back span belongs to a single-overhanging girder;
- The back span is subject to gravity loads only;
- Loads are applied at the top-flange level;
- OWSJs are equally spaced;
- All of the joist reactions are the same;
- Lateral deflections and twisting are prevented at support locations (fork supports);
- Warping deformation is allowed at support locations; and
- Torsional restraints coming from OWSJs are neglected.

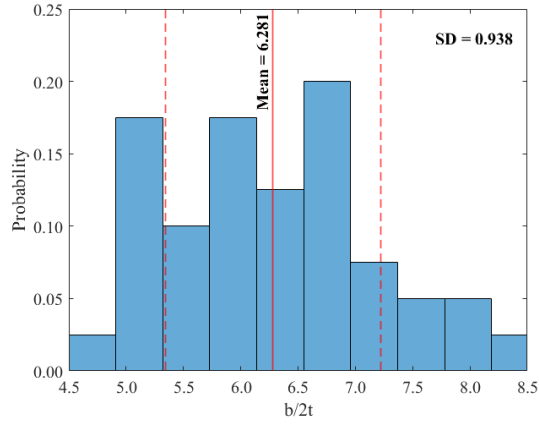
5. Summary and Conclusions

A comprehensive finite-element model capable of considering material and geometric nonlinearities, initial geometric imperfections, residual stresses, and distortions for overhanging girders with fork supports is developed. The results of the numerical simulation are proven to be in good agreement with the available experimental results.

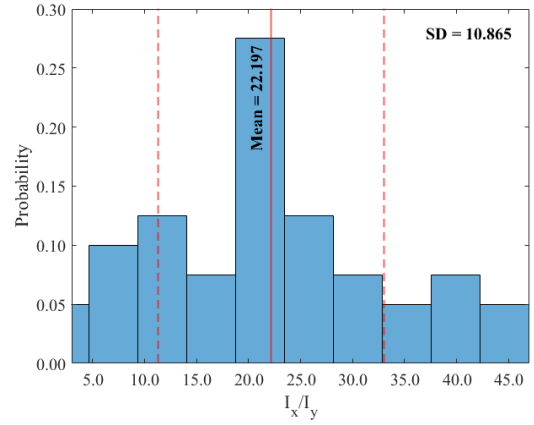
The validated numerical model is utilized to obtain the lateral–torsional buckling modification factors associated with the back spans of 19,200 different single-overhanging girders with top-flange bracing under the free-to-warp conditions, as is required for the use of interaction methods. The results are compared to the predictions of available design methods, from which the following observations emerge:

- Equations (2) and (3) provide overly conservative solutions when the back span is laterally restrained at the top flange level since they neglect to take into account the beneficial effect of top-flange bracing; and
- Equation (4) tends to overestimate the elastic critical moment of the back span.

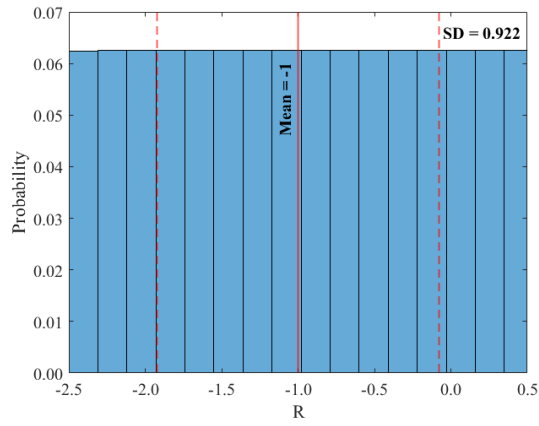
The support vector regression algorithm is applied to a dataset comprising the results of the 19,200 conducted numerical simulations to propose a model capable of predicting the lateral–torsional buckling modification factor of the back span of an arbitrary single-overhanging girder with top-flange bracing under the free-to-warp conditions based on only five dimensionless parameters: $b/2t$, I_x/I_y , R , n , and X . The mean numerical/predicted ratio is found to be 1.000 with a coefficient of variation of 1.3%. This promising achievement provides the groundwork for the development of a novel interaction design method for single-overhanging girders in the future.



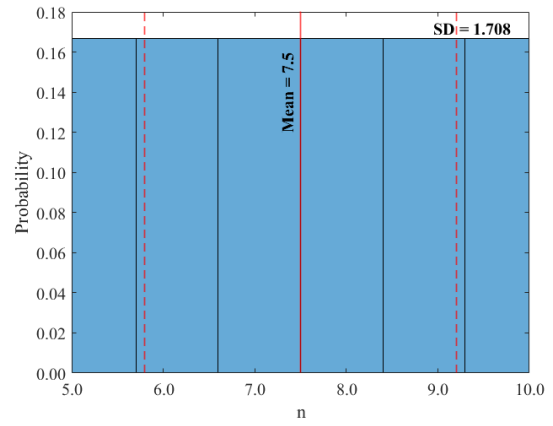
(a)



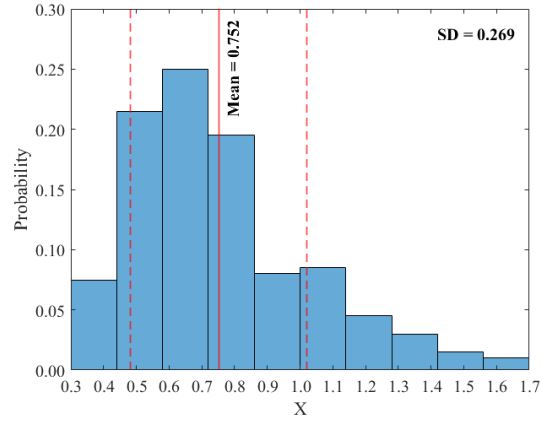
(b)



(c)



(d)



(e)

Figure 7: Probability distributions for selected features

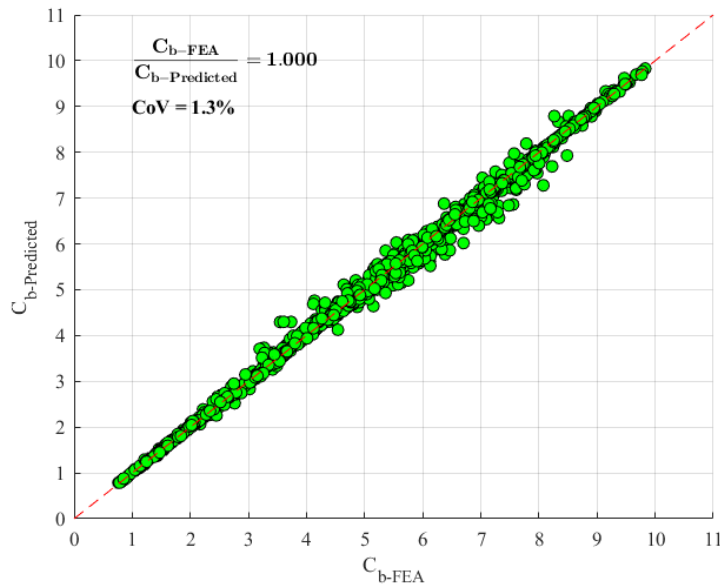


Figure 8: Performance of the proposed model

Acknowledgements

The financial assistance provided by the Natural Sciences and Engineering Research Council of Canada is greatly appreciated. The support provided by the Canadian Institute of Steel Construction (CISC) and the CISC Centre for Steel Structures Education and Research (the Steel Centre) at the University of Alberta is acknowledged.

References

- Albert, C., Essa, H. S., Kennedy, D. J. L. (1992). "Distortional buckling of steel beams in cantilever-suspended span construction," *Canadian Journal of Civil Engineering*, 19 (5) 767-780.
- American Institute of Steel Construction (AISC) (2016). "Specification for Structural Steel Buildings," *AISC 360-16*, AISC, Chicago, Illinois, The United States.
- Canadian Standards Association (CSA) (2019). "Design of Steel Structures," *CSA S16-19*, CSA, Toronto, Ontario, Canada.
- Dassault Systèmes (2017). "Abaqus/Standard User's Manual," *Version 2017*.
- Essa, H. S., Kennedy, D. J. L. (1993a). "Distortional buckling of steel beams," *Structural Engineering Report No. 185*, Department of Civil and Environmental Engineering, University of Alberta, Edmonton, Alberta, Canada.
- Essa, H. S., Kennedy, D. J. L. (1993b). "Bracing in cantilever-suspended span construction," *Proceedings of Structural Stability Research Council Conference*, Structural Stability Research Council, Lehigh University, Bethlehem, Pennsylvania, The United States.
- Essa, H. S., Kennedy, D. J. L. (1994). "Design of cantilever steel beams: refined approach," *Journal of Structural Engineering*, 120 (9) 2623-2636.
- Galambos, T. V (1998). "Guide to stability design criteria for metal structures," *Structural Stability Research Council*, John Wiley & Sons, New York, The United States.
- Kirby, P. A., Nethercot, D. A. (1979). "Design for structural stability," *Constrado Nomographs*, Granada Publishing, London, England.
- Mohri, M., Rostamizadeh, A., Talwalkar, A. (2018). "Foundations of machine learning," *The MIT Press*, Cambridge, Massachusetts, The United States.
- Nethercot, D. A. (1973) "The effective lengths of cantilevers as governed by lateral buckling," *The Structural Engineer*, 51 (5) 161-168.
- Rivas-Perea, P., Cota-Ruiz, J., Chaparro, D. G., Venzor, J. A. P., Carreon, A. Q., Rosiles, J. G. (2013). "Support vector

- machines for regression: a succinct review of large-scale and linear programming formulations,” *International Journal of Intelligence Science*, 3 5-14.
- Rongoe, J. (1996). “Design Guidelines for Continuous Beams Supporting Steel Joist Roof Structures,” *NASCC Proceedings*.
- Schmitke, C. D., Kennedy, D. J. L. (1985). “Effective lengths of laterally continuous, laterally unsupported steel beams,” *Canadian Journal of Civil Engineering*, 12 (3) 603-616.
- Trahair, N. S. (1983). “Lateral buckling of overhanging beams,” *Instability and Plastic Collapse of Steel Structures*, Granada Publishing, London, England.
- Vasios, N. (2015). “Nonlinear analysis of structures,” *Harvard University*, Cambridge, Massachusetts, The United States.
- Yura, J. A., Helwig, T. A. (2010). “Buckling of Beams with Inflection Points,” *Proceedings of the Annual Stability Conference*, Structural Stability Research Council, Orlando, Florida, The United States.
- Ziemian, R. D. (2010). “Guide to stability design criteria for metal structures,” *Structural Stability Research Council*, John Wiley & Sons, New York, The United States.